IEEE Photonics Journal
An IEEE Photonics Society Publication

Open Access

A Metal-Assisted Silicon Slot Waveguide for Highly Sensitive Gas Detection

Volume 9, Number 1, February 2017

Yuhei Ishizaka, *Member, IEEE*
Shuntaro Makino
Takeshi Fujisawa, *Member, IEEE*
Kunimasa Saitoh, *Member, IEEE*

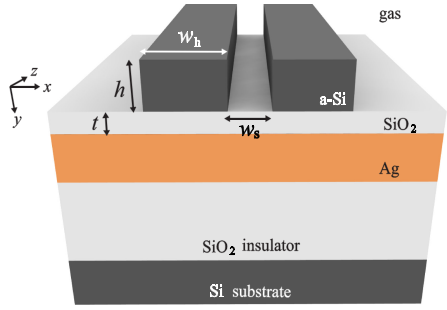

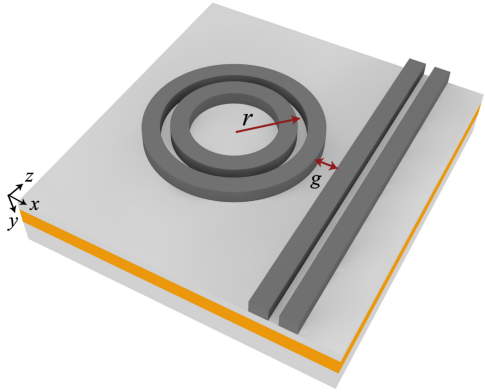

DOI: 10.1109/JPHOT.2016.2630308
1943-0655 © 2016 IEEE

IEEE photonics SOCIETY

IEEE

A Metal-Assisted Silicon Slot Waveguide for Highly Sensitive Gas Detection

Yuhei Ishizaka,[1,2] ***Member, IEEE*****, Shuntaro Makino,**[2]
Takeshi Fujisawa,[2] ***Member, IEEE*****,**
and Kunimasa Saitoh,[2] ***Member, IEEE***

[1]Department of Science and Engineering, Kanto Gakuin University
Yokohama 236-8501, Japan
[2]Graduate School of Information Science and Technology, Hokkaido University, Sapporo
060-0814, Japan

DOI:10.1109/JPHOT.2016.2630308

Manuscript received October 20, 2016; revised November 11, 2016; accepted November 12, 2016. Date of publication November 17, 2016; date of current version January 10, 2017. This work was supported in part by JSPS KAKENHI under Grant 15H06698. Corresponding author: Y. Ishizaka (e-mail: ishizaka@kanto-gakuin.ac.jp).

Abstract: A metal-assisted silicon slot waveguide for highly sensitive gas detection is proposed. To show the superiority of the proposed structure, the optical confinement factor in the gas region and the sensitivity are theoretically investigated using the 2-D vector finite element method. Numerical results show that the proposed structure can achieve a strong light confinement in the gas region compared with the conventional slot waveguide. The maximal optical confinement factor of 85% is obtained in the proposed structure, which is approximately 2.5 times larger than the conventional slot waveguide. Additionally, the results show that the proposed structure has a large sensitivity compared with the conventional slot waveguide. Finally, a ring resonator based on the proposed structure is analyzed to evaluate the *Q* factor and to increase the validity of results obtained by 2-D simulation.

Index Terms: Slot waveguides, surface plasmon polariton, finite element methods.

1. Introduction

Refractive index (RI) sensors have been investigated for several applications [1] such as gas detection and biochemical sensing [2]–[4]. To improve the sensitivity of these sensors, enhancement of the light-analyte interactions is important. Conventional studies [1]–[4] have shown that the use of slot waveguides [5] can strongly confine light to the low-index region filled with analyte.

Among the existing waveguides, nanoscale optical waveguides based on the surface plasmon polariton (SPP) have attracted the attention of researchers because the SPP mode is strongly localized in the nanoscale region. To date, various types of SPP-based waveguides have been reported; for example, metal-insulator-metal (MIM) waveguides [6], dielectric-loaded SPP waveguides [7], and hybrid plasmonic waveguides (HPWs) [8], [9]. HPWs achieve sub-wavelength confinement and are able to mitigate propagation loss. It is well known that the TM mode has been widely used in SPP-based waveguides because the excitation of the SPP mode relies on the TM mode. Conversely, it has been recently reported that the use of the TE mode in the polymer HPW has an advantage in the realization of the sharp bend [10]. In this case, by inserting a metal layer in an under cladding, the radiation of light to the region under the cladding can be suppressed. Additionally, the TE mode in the polymer-loaded SPP waveguide has been used for small bending

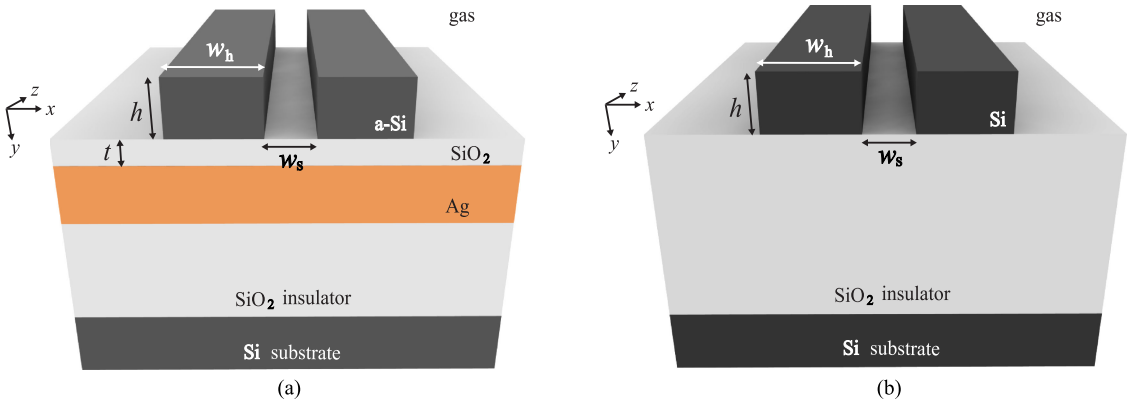

Fig. 1. Schematics of (a) a metal-assisted silicon slot waveguide and (b) a conventional silicon slot waveguide [1], [5]. The Si-width, slot width, and waveguide height are denoted as w_h, w_s, and h, respectively. The thickness of the SiO_2 layer is denoted as t. The over claddings of both slot waveguides are filled with acetylene gas.

with long propagation length [11]. In [11], such a TE mode was named the metal-assisted photonic mode. From the perspective of efficient bending, the use of the TE mode in the polymer-based SPP waveguides has an advantage compared with the use of the TM mode. This is because losses are given by the sum of the bending loss and the absorption loss due to the metal. Although the TE mode in SPP-based waveguides does not have a small field distribution compared with the TM mode, it has a longer propagation length. These studies suggest that the use of the TE mode in certain SPP-based waveguides would be useful for some applications.

In this paper, we propose a novel structure of a metal-assisted silicon slot waveguide for highly sensitive gas detection. In our structure, a metal layer is inserted as an under cladding to suppress the light confinement of the under cladding region, which leads to a strong light confinement in the gas region. In addition, the TE mode is used to confine light to the gas region. We evaluate the optical confinement factor and the sensitivity of the proposed structure and the conventional silicon slot waveguide using the 2-D vector finite element method (VFEM) [12]. Numerical results show that the proposed structure can achieve a strong light confinement in the gas region compared with the conventional slot waveguide. The maximal confinement factor of 85% is obtained in the proposed structure, which is approximately 2.5 times larger than for the conventional slot waveguide. Additionally, the results show that the proposed structure has a large sensitivity compared with the conventional slot waveguide. Finally, we analyze a ring resonator based on the proposed structure using the 3-D VFEM to evaluate the Q factor.

2. Metal-Assisted Silicon Slot Waveguide

2.1 Schematics of the Metal-Assisted Silicon Slot Waveguide

Figs. 1(a) and (b) show schematics of a metal-assisted silicon slot waveguide and a conventional silicon slot waveguide, respectively. In the proposed structure, a thin SiO_2 layer is sandwiched between Ag and silicon slot waveguides. We assume that the over claddings are filled with acetylene gas in both slot waveguides, and the refractive indexes of amorphous Si (a-Si), Si, SiO_2, acetylene gas, and Ag are 3.455, 3.455, 1.445, 1.000593 [1], and $0.1453 - j11.3587$ [9], respectively. In the metal-assisted slot waveguide, the core material is assumed to be a-Si because our structure is multilayered. The Si-width, slot width, and waveguide height are denoted as w_h, w_s, and h, respectively. The thickness of the SiO_2 layer is denoted as t. All the 2-D simulations are conducted with the wavelength of 1550 nm. Our proposed structure is compatible with existing CMOS fabrication processes and can be constructed as follows: After the Ag layer is coated on the Si wafer with the SiO_2 layer, amorphous silicon is deposited onto the SiO_2 surface [13]. Then,

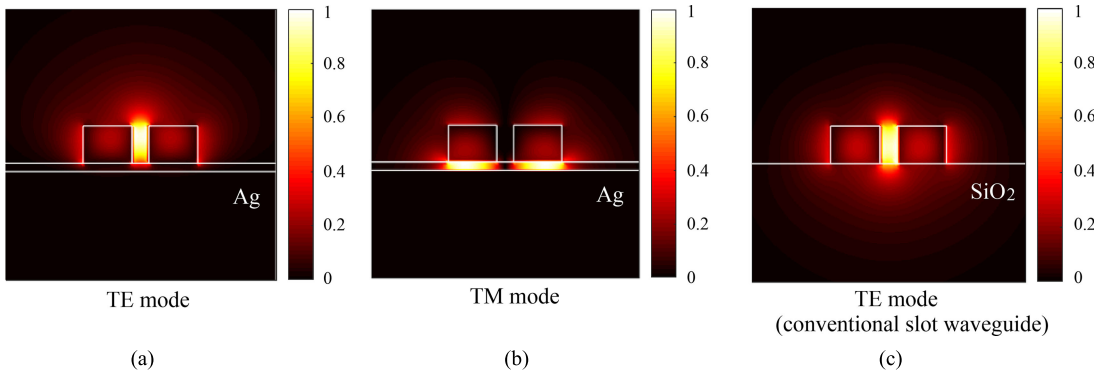

Fig. 2. Electric field distributions of the metal-assisted silicon slot waveguide for (a) the TE mode and (b) the TM mode. (c) Electric field distribution of the TE mode for the conventional slot waveguide. The light confinement of the under cladding region in the proposed structure is weaker than the conventional slot waveguide. The light concentration in the gas region shown in (a) is remarkable compared with the TM mode shown in (b).

the amorphous silicon layer is etched to form a slot waveguide. Figs. 2(a) and (b) show the electric field distributions of the metal-assisted silicon slot waveguide ($w_h = 0.29\,\mu$m, $w_s = 0.1\,\mu$m, $h = 0.22\,\mu$m, $t = 0.05\,\mu$m) for the TE mode and the TM mode, respectively. For the TE mode that is used in our structure, the light concentration in the gas region is remarkable compared with the TM mode that has been frequently used in SPP-based waveguides. Fig. 2(c) shows the electric field distribution of the conventional silicon slot waveguide ($w_h = 0.29\,\mu$m, $w_s = 0.1\,\mu$m, $h = 0.22\,\mu$m). We can see that the light confinement of the under cladding region in the proposed structure is weaker than the conventional slot waveguide. This characteristics facilitates a large confinement of light in the over cladding. A detailed investigation is shown in Section 2.2.

2.2 Model Investigation

Because the sensitivity of RI sensors is proportional to the optical confinement factor [1], a large light confinement in the over cladding leads to the improvement of the sensor sensitivity. When the optical confinement factor is large, the effective refractive index is strongly affected by the concentration change of a cover medium such as aqueous solution or gas. When considering an RI sensor based on a ring resonator, the concentration change of gas affects shifts in the resonant wavelength of ring resonators, which can be expressed as [1]

$$\Delta\lambda = \lambda_0 \left(\frac{\Gamma}{n_{\text{eff}}} \right) \Delta n_{\text{gas}} \tag{1}$$

where λ_0 is the unperturbed resonant wavelength, and n_{eff} is the unperturbed value of the effective refractive index. Γ is the optical confinement factor in the gas region, which is given by the following equation [14]:

$$\Gamma = \frac{\int\int_{\text{gas}} \text{Re}\,(\boldsymbol{E} \times \boldsymbol{H}^*) \cdot \boldsymbol{i}_z dxdy}{\int\int_{\text{total}} \text{Re}\,(\boldsymbol{E} \times \boldsymbol{H}^*) \cdot \boldsymbol{i}_z dxdy} \tag{2}$$

where $\boldsymbol{E}$ and $\boldsymbol{H}$ are the electric field vector and the magnetic field vector, respectively, and $*$ denotes the complex conjugate. The integrals are calculated inside the gas region and the entire cross section region. Note that we use the optical confinement factor considering the electric field of the z component because high-index-contrast waveguides such as silicon slot waveguides have a large electric field of z component [15]. We investigate the performances of the proposed structure using the 2-D VFEM. The model is analyzed by changing w_h and w_s when $h = 0.22\,\mu$m and $t = 0.05\,\mu$m.

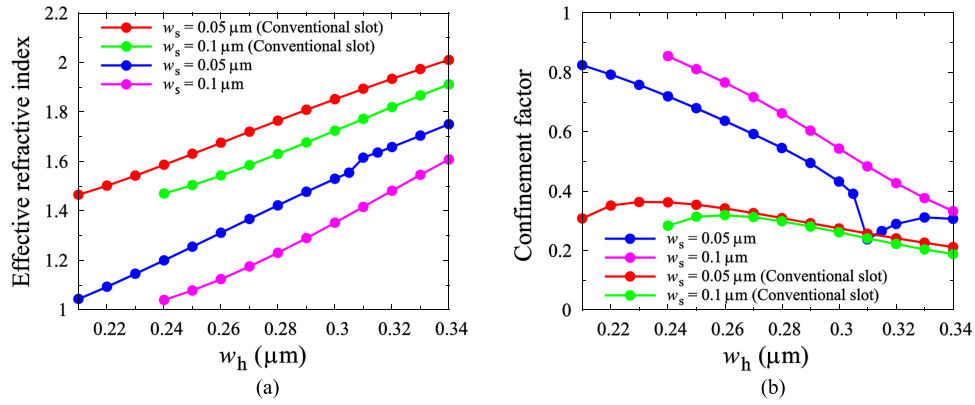

Fig. 3. (a) Effective refractive index and (b) the optical confinement factor as a function of w_h when $h = 0.22\,\mu$m and $t = 0.05\,\mu$m. The blue and purple lines represent results for the proposed structures, while the red and green lines represent results for the conventional slot waveguides.

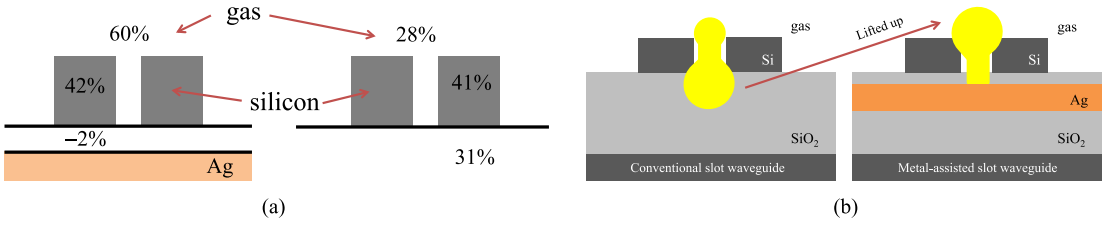

Fig. 4. (a) Power distributions of the metal-assisted silicon slot waveguide and the conventional silicon slot waveguide. (b) Mechanism of a strong light confinement in the over cladding filled with gas. The yellow regions represent the light concentration.

Fig. 3(a) shows the effective refractive index n_{eff} of the metal-assisted silicon slot waveguide and the conventional silicon slot waveguide as a function of the Si-width w_h. The effective refractive index increases as the Si-width of the slot waveguides increases. In general, the mode is radiated if the real prat of the effective refractive index is under the second-largest refractive index. For the photonic slot waveguide without metal, because SiO_2 is a material with the second-largest refractive index, the cut-off condition is defined as the real part of $n_{\text{eff}} < 1.445$. For the proposed structure with metal, acetylene gas is a substantial material with the second-largest refractive index because light reflects at the metal layer with the thin SiO_2 layer. In this case, the cut-off condition is defined as the real part of $n_{\text{eff}} < 1.000593$. Here, we emphasize that the all the plotted points including $n_{\text{eff}} < 1.445$ of the blue and purple lines indicate guided modes. Fig. 3(b) shows the optical confinement factor in the gas region of both slot waveguides as a function of the Si-width. Note that a rapid decline of the optical confinement factor at $t = 0.31\,\mu$m for the blue line is due to mode coupling between the TE mode and the TM mode (detailed discussions are provided in section 3). The optical confinement factor of the metal-assisted silicon slot waveguide is larger than that of the conventional slot waveguide. The maximal confinement factor of 85% is obtained in the proposed structure when $w_h = 0.24\,\mu$m and $w_s = 0.1\,\mu$m, while the maximal confinement factor is only 36% in the conventional structure when $w_h = 0.23\,\mu$m and $w_s = 0.05\,\mu$m. To further examine this result, the power distributions of both slot waveguides in the case of $w_h = 0.29\,\mu$m are depicted in Fig. 4(a). First, the powers of both waveguides in the Si region are almost same. The powers of the proposed structure and the conventional structure are 42% and 41%, respectively. Second, for the proposed structure, the power under the cladding is −2% although the power of the conventional structure under the cladding is 31%. Note that the negative value in Fig. 4(a) indicates the back propagation of light near the metal [16]. Thus, inserting a metal layer reduces the light

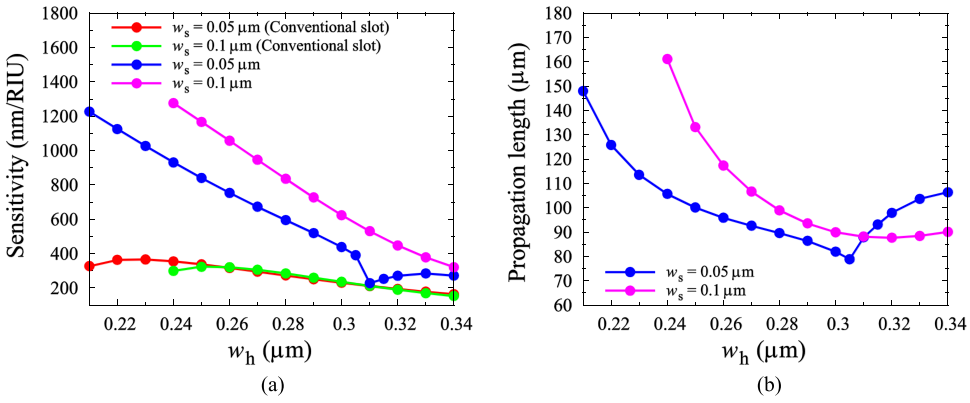

Fig. 5. (a) Sensitivity and (b) the propagation length as a function of w_h when $h = 0.22\,\mu$m and $t = 0.05\,\mu$m.

confinement in the under cladding region. As a result, the light confinement in the gas region of the proposed structure becomes larger than that of the conventional structure. The achievement of a strong light confinement is due to a large reflection by the metal. Fig. 4(b) describes the mechanism of a strong light confinement in the over cladding filled with gas.

Because the sensitivity of the device is determined by the ratio between the shift in the resonant wavelength and the shift in the refractive index of the gas, we evaluate the values of $\lambda_0\Gamma/n_{\text{eff}}$ (nm/RIU). This sensitivity measure is derived from (1). Fig. 5(a) shows the sensitivity of both slot waveguides as a function of the Si-width w_h when assuming $\lambda_0 = 1550$ nm. From Fig. 5(a), we find that the sensitivity of the proposed structure exceeds 1000 nm/RIU. This value is more than two times as large as the sensitivity of the conventional slot waveguide. As metal is introduced in the proposed structure, it is necessary to estimate the propagation loss due to the optical absorption in the metal. Fig. 5(b) shows the propagation length as a function of the Si-width. The propagation length L_{prop}, which is determined by the condition that light intensity attenuates to $1/e$, is given by

$$L_{\text{prop}} = \frac{1}{|2\text{Im}(\beta)|} \tag{3}$$

where β is the propagation constant. From Fig. 5(b), we can see that the range of the propagation length is from 80 μm to 160 μm.

3. Influence of the SiO_2 Thickness

The distance between the core region and the Ag layer is the key parameter to determine the effect of light confinement in the gas region, thus, the influence of the SiO_2 thickness is investigated in this section. Fig. 6(a) shows the effective refractive index as a function of t when $w_s = 0.1\,\mu$m. We can see that the effective refractive index increases as t increases. As t increases, our structure approaches the conventional slot waveguide. Figs. 6(b) and (c) show the optical confinement factor and the sensitivity with respect to t when $w_s = 0.1\,\mu$m. The sensitivity is defined as $\lambda_0\Gamma/n_{\text{eff}}$ (nm/RIU). These graphs are similar because the optical confinement factor is proportional to the sensitivity. The optical confinement factor and the sensitivity decrease as t increases because the effect of metal reflection becomes basically decreases. In addition, rapid declines are observed at $t = 0.12\,\mu$m and $w_h = 0.26\,\mu$m (see red line) and at $t = 0.09\,\mu$m and $w_h = 0.3\,\mu$m (see green line). Fig. 6(d) shows the propagation length as a function of t when $w_s = 0.1\,\mu$m. Because the structure is approaching the conventional slot waveguide as t increases, losses due to the metal are gradually reduced. For example, the propagation length is approximately 1000 μm in the case of $t = 0.3$ and $w_h = 0.26\,\mu$m.

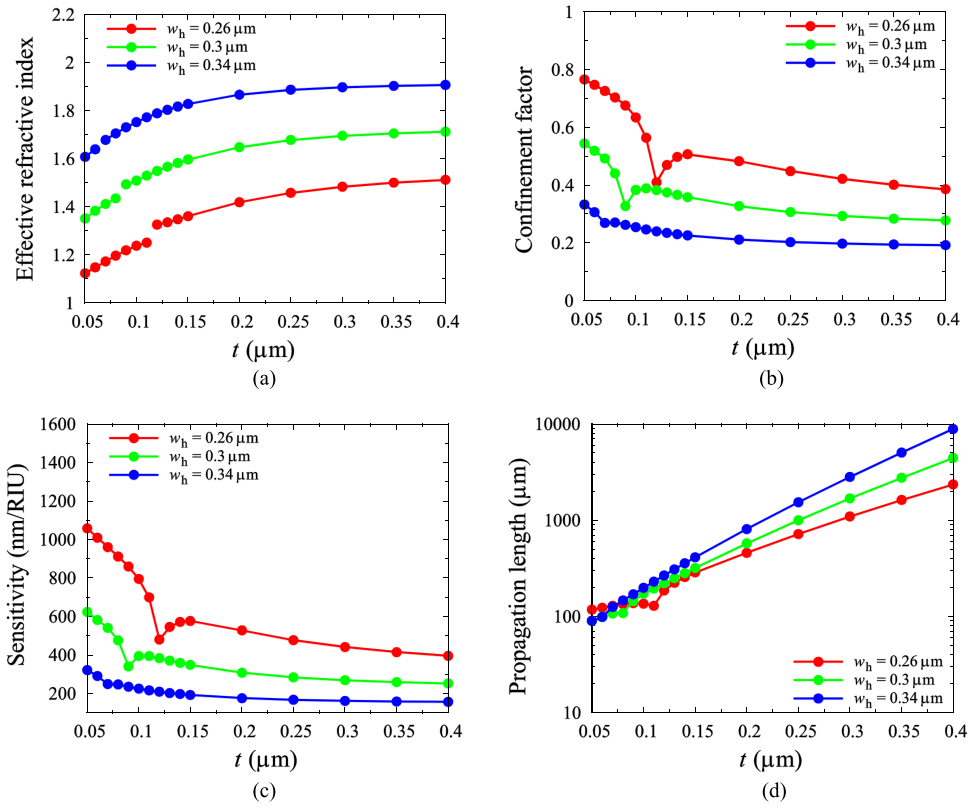

Fig. 6. (a) Effective refractive index, (b) the optical confinement factor, (c) the sensitivity, and (d) the propagation length as a function of t when $w_s = 0.1\,\mu$m.

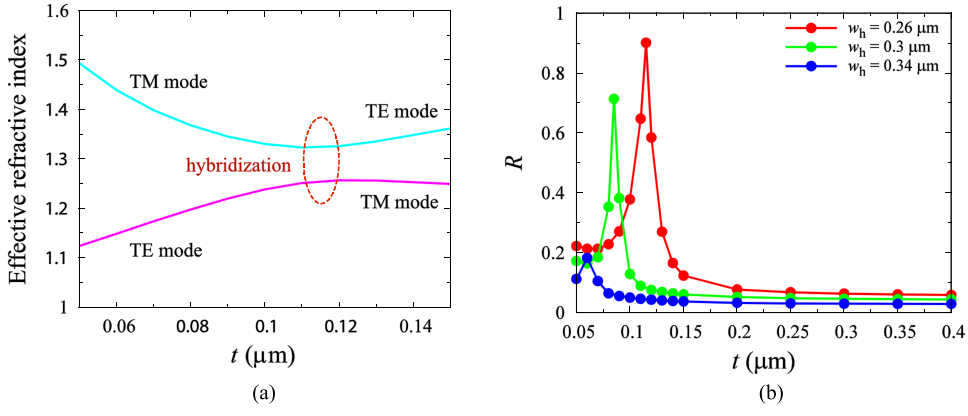

Fig. 7. (a) Anti-crossing associated with mode coupling between the TE mode and the TM mode. (b) Hybridization of the TE mode and the TM mode as a function of the thickness of the SiO_2 layer t, where R is the ratio between the E_x component and the E_y component in the whole of the x-y section.

To investigate the cause of the rapid declines of the optical confinement factor and the sensitivity at specific values of t in Figs. 6(b) and (c), we evaluate the effective refractive index of the TE and TM modes around $t = 0.12\,\mu$m when $w_h = 0.26\,\mu$m, as shown in Fig. 7(a). From Fig. 7(a), it is confirmed that anti-crossing associated with mode coupling between the TE mode and the TM mode occurs. To evaluate the mode coupling quantitatively, the hybridization ratio R of the TE mode

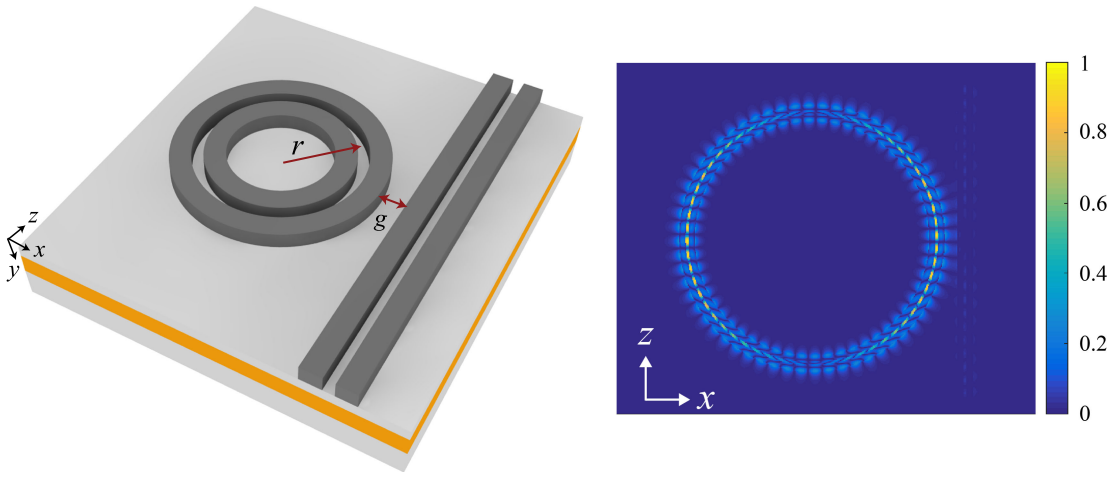

(a) (b)

Fig. 8. (a) Schematic of a ring resonator based on the metal-assisted slot waveguide, where the radius of the ring and the gap between the bus waveguide and the ring are denoted as r and g, respectively. (b) Electric field distribution for $|E_x|$.

and the TM mode is investigated in the proposed structure. Fig. 7(b) shows the hybridization ratio R as a function of t, where R indicates the ratio between the E_x component and the E_y component in the whole of the x-y section. The definition of R is given as follows [17]:

$$R = \frac{\iint n^2(x,y)\, E_y^2(x,y)\, dxdy}{\iint n^2(x,y)\, E_x^2(x,y)\, dxdy}, \quad 0 \le R \le 1 \tag{4}$$

where n is the refractive index, and E_x and E_y are the electric fields of the x component and the y component, respectively. From Fig. 7(b), it can be seen that mode coupling occurs between the TE and TM modes at around $t = 0.12\,\mu$m when $w_h = 0.26\,\mu$m. If we use the proposed structures for RI sensors, parameters that have a large R should not be selected to avoid the hybridization, which leads to degradation of the sensitivity.

4. 3-D Simulation of the Ring Resonator and Discussion

Fig. 8(a) shows a schematic of a ring resonator based on the proposed slot waveguide. In the ring structure, the radius of the ring and the gap between the bus waveguide and the ring are denoted as r and g, respectively. To evaluate the sensitivity and the Q factor of the ring resonator, the 3-D VFEM for the cavity problem is employed. Applying the finite element method as in the case of [18], we obtain a final matrix equation as follows:

$$[K]\{\phi\} = \left(\frac{\omega_0}{c}\right)^2 [M]\{\phi\} \tag{5}$$

where $[K]$ and $[M]$ are finite element matrices and $\{\phi\}$ is an edge valuable vector of unknown electric/magnetic fields. These matrices and vectors are described in detail in [18] and [19]. Additionally, ω_0 and c are the resonant angular frequency and the speed of light, respectively. Since the 3-D VFEM is a frequency domain analysis, the Q factor is calculated by the following equation:

$$Q = \frac{\mathrm{Re}(\omega_0)}{2\mathrm{Im}(\omega_0)}. \tag{6}$$

In our 3-D simulation, parameters are set as $r = 5\,\mu$m, $g = 0.5\,\mu$m, $w_s = 0.1\,\mu$m, $w_h = 0.26\,\mu$m, and $h = 0.22\,\mu$m. To estimate the sensitivity, we analyzed the ring resonator twice by

TABLE 1
Simulation results of the ring resonator with metal when $t = 0.2\,\mu$m and $t = 0.4\,\mu$m. The sensitivity for 3-D simulation is calculated by $\Delta\lambda/\Delta n_{gas}$

t (μm)	n_{gas}	Q factor	Resonant wavelength λ (nm)	Sensitivity (nm/RIU) (3-D simulation)	Sensitivity (nm/RIU) (2-D simulation)
0.2	1.000593	4700	1544.59	458	527
	1.020593	4600	1553.74		
0.4	1.000593	3900	1542.06	394	395
	1.020593	3200	1549.94		

changing the refractive index of acetylene gas n_{gas}. Fig. 8(b) shows an obtained electric field distribution ($|E_x|$) for the ring resonator with $t = 0.2\,\mu$m. From Fig. 8(b), it is confirmed that light is confined in the ring. Table 1 shows simulation results of the ring resonator with metal when $t = 0.2\,\mu$m and $t = 0.4\,\mu$m. For $t = 0.2\,\mu$m, the sensitivity of 458 nm/RIU is obtained by 3-D simulation. In contrast, the sensitivity of 527 nm/RIU is obtained by 2-D simulation (see section 3). Similarly, in the case of $t = 0.4\,\mu$m, the sensitivity of 394 nm/RIU is obtained by 3-D simulation and the sensitivity of 395 nm/RIU is obtained by 2-D simulation. From these results, it is determined that estimation of the sensitivity from (1) is sufficiently useful for the proposed structure with the metal layer. In addition, the Q factor of approximately 4600 is obtained when $t = 0.2\,\mu$m.

Here, we discuss the insertion loss and the coupling between the bus waveguide and the ring when inserting the metal layer. In the case of a small t, the insertion loss will increase because of the metal loss. However, with a large t, the metal loss does not greatly affect the insertion loss. For example, the metal loss of the proposed structure with $t = 0.2\,\mu$m is 0.009 dB/μm. In this case, if we construct a ring resonator with 5 μm radius and 10 μm bus waveguide, the increase of loss is approximately 0.37 dB compared with the ring resonator without the metal. Form the theoretical point of view, the coupling length is determined by the overlap of the evanescent fields in two parallel optical waveguides. Even for a hybrid plasmonic waveguide with a metal layer, the coupling mechanism does not change [20]. Nevertheless, the coupling length will be changed. The coupling length of our structure is considered to be longer than that of the conventional slot waveguide. This is because the overlap of the evanescent fields in the under cladding decreases, which leads to a longer coupling length. Incidentally, for an all-pass ring resonator, a weak coupling tends to manifest a high Q value [21]. This implies that a longer coupling length has an advantage in terms of the Q value.

5. Conclusion

We have proposed a metal-assisted silicon slot waveguide to obtain strong light confinement in the low-index region for highly sensitive gas detection. In our structure, the metal layer is inserted to suppress the light confinement of the under cladding region, which leads to a strong light confinement in the gas region. We have evaluated the optical confinement factors of the proposed structure and the conventional silicon slot waveguide using the 2-D VFEM. Numerical results show that the proposed structure can achieve a strong light confinement in the gas region compared with the conventional slot waveguide. The maximal confinement factor of 85% is obtained in the proposed structure, which is approximately 2.5 times larger than that of the conventional slot waveguide. Additionally, the results show that the proposed structure has a large sensitivity compared with the conventional slot waveguide. In addition to this, we clarify that the mode coupling that deteriorates the sensitivity occurs between the TE mode and the TM mode at specific structures. To avoid

this, parameters that have a large hybridization ratio should not be selected when constructing RI sensors. Finally, we analyze a ring resonator based on the proposed structure using the 3-D VFEM for the cavity problem to evaluate the *Q* factor. The 3-D simulation shows that the *Q* factor of approximately 4600 is obtained. From the result of the sensitivity evaluated by 3-D analysis, it is determined that estimating the sensitivity from the optical confinement factor is sufficiently useful for the proposed structure with the metal layer. Future areas of study include the detailed design of cavities and experimental verification of the benefits of our structure for implementation of a highly sensitive gas detector.

References

[1] J. T. Robinson, L. Chen, and M. Lipson, "On-chip gas detection in silicon optical microcavities," *Opt. Exp.*, vol. 16, no. 6, pp. 4296–4301, Mar. 2008.
[2] F. Dell'Olio and V. M. Passaro, "Optical sensing by optimized silicon slot waveguides," *Opt. Exp.*, vol. 15, no. 8, pp. 4977–4993, Apr. 2007.
[3] C. A. Barrios *et al.*, "Slot-waveguide biochemical sensor," *Opt. Lett.*, vol. 32, no. 21, pp. 3080–3082, Nov. 2007.
[4] Q. Liu, J. S. Lee, and M. K. Park, "A refractive index sensor design based on grating-assisted coupling between a strip waveguide and a slot waveguide," *Opt. Exp.*, vol. 21, no. 5, pp. 5897–5909, Mar. 2013.
[5] V. R. Almeida, Q. Xu, C. A. Barrios, and M. Lipson, "Guiding and confining light in void nanostructure," *Opt. Lett.*, vol. 29, no. 11, pp. 1209–1211, Jun. 2004.
[6] J. A. Dionne, L. A. Sweatlock, and H. A. Atwater, "Plasmon slot waveguides: Towards chip-scale propagation with subwavelength-scale localization," *Phys. Rev. B*, vol. 73, no. 3, pp. 035407-1–035407-9, Jan. 2006.
[7] A. V. Krasavin and A. V. Zayats, "Silicon-based plasmonic waveguides," *Opt. Exp.*, vol. 18, no. 11, pp. 11791–11799, May 2010.
[8] M. Z. Alam, J. Meier, J. S. Aithison, and M. Mojahedi, "Super mode propagation in low index medium," in *Proc. Quantum Electron. Lasers Sci. Conf.*, May 2007, Paper JThD112.
[9] R. F. Oulton, V. J. Sorger, D. A. Genov, D. F. P. Pile, and X. Zhang, "A hybrid plasmonic waveguide for subwavelength confinement and long-range propagation," *Nature Photon.*, vol. 2, no. 8, pp. 496–500, Aug. 2008.
[10] M. A. Sefunc, M. Pollnau, and S. M. García-Blance, "Low-loss sharp bends in polymer waveguides enabled by the introduction of a thin metal layer," *Opt. Exp.*, vol. 21, no. 24, pp. 29808–29817, Nov. 2013.
[11] C. Yang, E. J. Teo, T. Goh, S. L. Teo, J. H. Teng, and A. A. Bettiol, "Metal-assisted photonic mode for ultrasmall bending with long propagation length at visible wavelengths," *Opt. Exp.*, vol. 20, no. 21, pp. 23898–23905, Oct. 2012.
[12] K. Saitoh and M. Koshiba, "Full-vectorial imaginary-distance beam propagation method based on a finite element scheme: Application to photonic crystal fibers," *IEEE J. Quantum Electron.*, vol. 38, no. 7, pp. 927–933, Jul. 2002.
[13] R. Sun *et al.*, "Horizontal single and multiple slot waveguides: Optical transmission at $\lambda = 1550$ nm," *Opt. Exp.*, vol. 15, no. 26, pp. 17967–17972, Dec. 2007.
[14] N.-N. Feng, J. Michel, and L. C. Kimerling, "Optical field concentration in low-index waveguides," *IEEE J. Quantum Electron.*, vol. 42, no. 9, pp. 885–890, Sep. 2006.
[15] J. B. Driscoll, X. Liu, S. Yasseri, I. Hsieh, J. I. Dadap, and R. M. Osgood, Jr., "Large longitudinal electric field (Ez) in silicon nanowire waveguides," *Opt. Exp.*, vol. 20, no. 21, pp. 2797–2804, Aug. 2009.
[16] D. Y. Fedyanin, A. V. Arsenin, V. G. Leiman, and A. D. Gladun, "Backward waves in planar insulator-metal-insulator waveguide structures," *J. Opt.*, vol. 12, no. 1, pp. 015002-1–015002-7, Nov. 2009.
[17] V. P. Tzolov and M. Fontaine, "A passive polarization converter free of longitudinally-periodic structure," *Opt. Commun.*, vol. 127, no. 1/3, pp. 7–13, Jun. 1996.
[18] Y. Ishizaka, Y. Kawaguchi, K. Saitoh, and M. Koshiba, "Three-dimensional finite-element solutions for crossing slot-waveguides with finite core-height," *Lightw. Technol.*, vol. 30, no. 21, pp. 3394–3400, Nov. 2012.
[19] S. Makino, T. Sato, Y. Ishizaka, T. Fujisawa, and K. Saitoh, "Three-dimensional finite-element time-domain beam propagation method and its application to 1-D photonic crystal-coupled resonator optical waveguide," *J. Lightw. Technol.*, vol. 33, no. 18, pp. 3836–3842, Sep. 2015.
[20] M. Nagai, Y. Ishizaka, K, Saitoh, and M. Koshiba, "Propagation length and coupling characteristics of a hybrid plasmonic waveguide with a uniform silica layer," in *Proc. Conf. Lasers Electro-Opt. Pacific Rim*, 2013, Paper TuPI-16.
[21] W. Bogaerts *et al.*, "Silicon microring resonators," *Laser Photon. Rev.*, vol. 6, no. 1, pp. 47–73, 2012.